arXiv:cond-mat/0306657v1 [cond-mat.mtrl-sci] 25 Jun 2003

Theory of pattern-formation of metallic microparticles in poorly conducting liquid

I. S. Aranson[1] and M. V. Sapozhnikov[1,2]
[1] *Materials Science Division, Argonne National Laboratory, 9700 South Cass Avenue, Argonne, IL 60439*
[2] *Institute for Physics of Microstructures, Russian Academy of Sciences, GSP-105, Nizhny Novgorod, 603000, Russia*
(Dated: February 2, 2008)

We develop continuum theory of self-assembly and pattern formation in metallic microparticles immersed in a poorly conducting liquid in DC electric field. The theory is formulated in terms of two conservation laws for the densities of immobile particles (precipitate) and bouncing particles (gas) coupled to the Navier-Stokes equation for the liquid. This theory successfully reproduces correct topology of the phase diagram and primary patterns observed in the experiment [Sapozhnikov et al, Phys. Rev. Lett. **90**, 114301 (2003)]: static crystals and honeycombs and dynamic pulsating rings and rotating multi-petal vortices.

PACS numbers: 45.70.Qj,05.65.+b,47.15.Cb,47.55.Kf

Electromagnetic manipulation and assembly of small particles in electrolytes has constitutes one of the great hopes for nanotechnology [1] and new generation of microfluidic devices [2]. Many industrial technologies face the challenge of handling such single- or multi-component micro and nano- size ensembles. The dynamics of conducting microparticles in electric field in the air was studied in [3, 4]. Phase transitions and clustering instability of the electrostatically driven conducting microparticles were found. In our recent work we reported new dynamic phenomena occurring with microparticles in poorly conducting liquid subject to strong electric field (up to 20 kV/cm) [5]. It was shown that small metallic particles immersed in a toluene-ethanol mixture in DC electric field form a rich variety of novel phases. These phases include static honeycombs and two-dimensional crystals; dynamic multi-petal vortices and pulsating rings. The phenomena were attributed to interaction between particles and electro-hydrodynamic (EHD) flows.

In this Letter we develop theory of pattern formation and self-assembly of metallic microparticles in a poorly conducting liquid placed between two horizontal planar electrodes. The theory is formulated in terms of two depth-averaged conservation laws for the densities of immobile particles (precipitate) and bouncing particles (gas) coupled to the Navier-Stokes equation for vertical component of velocity of the liquid v_z, whereas horizontal velocity $v_\perp$ is obtained from the continuity condition. This theory successfully reproduces topology of the phase diagram and primary patterns observed in the experiment: static crystals and honeycombs and dynamic pulsating rings and vortices [5]. In the framework of our theory we demonstrate that the rotation of clusters is the result of a symmetry-breaking instability leading to formation of the travelling wave at the cluster perimeter.

Model. Schematics of experimental setting is shown in inset of Figure 1. Our studies show that two major control parameters are the potential difference ΔU which determines average electric field $E = -\Delta U/d$, d is the spacing between electrodes, and the concentration c of the additive (e.g. ethanol) which characterizes the conductivity of the liquid. Following the analysis of Ref. [4], we describe the evolution of particulate by the number density of precipitate $\rho_p(\mathbf{r}, t)$ and bouncing particles (or gas) $\rho_g(\mathbf{r}, t)$, where $\mathbf{r} = (x, y)$ are horizontal coordinates. All the quantities are averaged over the vertical coordinate z. Since the total number of particles $N = \int(\rho_p + \rho_g)dxdy$ is conserved, the evolution of the particulate is described by the conservation laws

$$\partial_t \rho_p = \nabla \mathbf{J}_p + f \ , \ \partial_t \rho_g = \nabla \mathbf{J}_g - f \qquad (1)$$

Here $J_{p,g}$ are the mass fluxes of precipitate and gas respectively and the function f describes gas/precipitate conversion which depends on $\rho_{p,g}$, electric field E and local concentration c. The fluxes can be written as:

$$\mathbf{J}_{p,g} = D_{p,g}\nabla\rho_{p,g} + \alpha_{p,g}(E)\mathbf{v}_\perp\rho_{p,g}(1 - \beta(E)\rho_{p,g}) \qquad (2)$$

where $D_{p,g}$ are precipitate/gas diffusivities. The last term, describing particles advection by fluid, is reminiscent of Richardson-Zaki relation for drag force frequently used in the engineering literature [6]. The factor $(1 - \beta(E)\rho_{p,g})$ describes saturation of the flux at large particle densities $\rho \sim 1/\beta$. Experiments show that at the onset of motion the maximum density in the patterns such as honeycombs is below sub-monolayer coverage whereas for large values of E the particles form multi-layered structures. Thus β should decrease with the increase of E. According to the Richardson-Zaki relation, the coefficients $\alpha_{g,p}$ decrease with the increase of $\rho_{g,p}$ (i.e. void fraction). In order to mimic this effect on qualitative level we assumed that $\alpha_{g,p}$ decreases with the increase of E (due to the increase of maximum density $\rho \sim 1/\beta$ with E). Since the gas is mostly concentrated near the upper electrode and the precipitate near the bottom, gas and precipitate are advected in *opposite directions*, i.e. the transport coefficients $\alpha_{p,g}$ have opposite signs. Since gas is more mobile than precipitate, we set $D_g \gg D_p$. In the limit $D_g \to \infty$ and for $\alpha_{p,g} = 0$ one recovers the description of Ref. [4].

We assume that vertical vorticity of the liquid $\Omega_z = \partial_x v_y - \partial_y v_x$ is small in comparison with the in-plane vorticity. This assumption is justified by the experimental observation that toroidal vortices create no or very small horizontal rotation. From $\Omega_z = 0$ one obtains

$$\mathbf{v}_\perp = -\nabla\phi \tag{3}$$

where ϕ is a "quasipotential". Substituting Eq. (3) into the continuity equation $\nabla\mathbf{v} = 0$ one expresses the quasipotential through vertical velocity

$$\nabla^2\phi = \partial_z v_z \tag{4}$$

The vertical velocity v_z can be obtained form the corresponding Navier-Stokes equation

$$\rho_0(\partial_t v_z + \mathbf{v}\nabla v_z) = \nu\nabla^2 v_z - \partial_z p + E_z q \tag{5}$$

where ρ_0 is the density of liquid (we set $\rho_0 = 1$), ν is the viscosity, p is the pressure, and q is the charge density. The last term describes electric force acting on charged liquid. In order to average Eqs. (4),(5) over the thickness of the cell $0 < z < d$, we assume that v_z is symmetric with respect to $d/2$ and $v_\perp$ is antisymmetric. Then after the averaging and taking into account that $\partial_z v_z = 0$ at $z = 0, d$ one obtains

$$\partial_t V = \nu\nabla^2 V - \zeta V - \Delta p + \langle E_z q\rangle \tag{6}$$

where $V = d^{-1}\int_0^d v_z dz$, and $\Delta p = p(d) - p(0)$. Term $-\zeta V$ accounts for a small dissipation due to friction between liquid, particles, and the walls of container. Using the symmetry condition and integrating Eq. (4) over the lower half of the cell $(0 < z < d/2)$ one obtains

$$\nabla^2\Phi = a_0 V \tag{7}$$

where the constant $a_0 \sim O(1)$ can be scaled away and Φ is averaged ϕ. The volume charge density $q \sim -c$ is negative and proportional to additive concentration c, vertical component of the electric field E_z depends on E and the local density of particles, $\rho_p + \rho_g$. Since the increase in the amount of conducting particles decreases the effective spacing between the electrodes and, therefore, increases the apparent electric field, one obtains

$$E_z \approx \frac{E}{1 - (\rho_p + \rho_g)/s} \sim E + E(\rho_p + \rho_g)/s \tag{8}$$

where constant $s \approx d/r_0$, r_0 is particle diameter. After applying the divergence operator to the Navier-Stokes equation one finds that the pressure itself is a functional of $\langle Eq\rangle$. In the most general form it can be written as $\Delta p = \int K(r - r')\langle E_z q\rangle dr'$. The kernel has property $\int K dr' = 1$ since uniform force distribution does not create net flow of the liquid. The precise form of the kernel

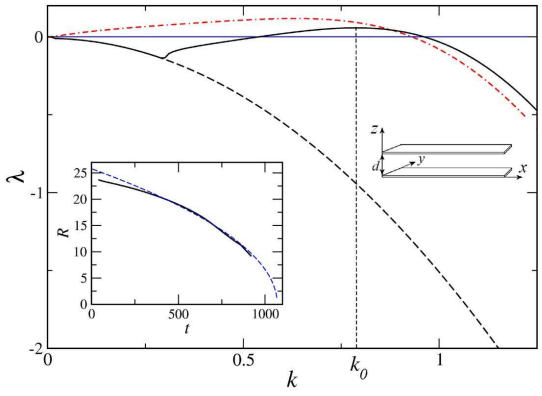

FIG. 1: Real part of λ vs k for three regimes: honeycomb (solid line, $E = -45, \beta = 2, \kappa = -0.1$), coalescence (point-dashed line $E = -55, \beta = 0.5, \kappa = 0.1$), stable 2D crystal (dashed line, $E = 50, \beta = 2, \kappa = -0.1$). Other parameters: $\zeta = 0.02, \bar{\rho} = 0.3, D_p = 1, \alpha_p = \alpha_g = -0.3, \nu = 2, d_0 = 1, \mu_0 = 0$. Inset: Schematics of experimental setup (right) and distance R between t-vortices vs t (solid line) for parameters of Figure 4 (left). Dashed line shows fit $R \sim \sqrt{t_0 - t}$.

is not available on our level of description. We used the following kernel expressed by its Fourier transform

$$\hat{K}(k) = \int \exp[i\mathbf{kr}]K(r)dr = \exp[-\kappa(E)k^2 - k^4 d_0^4] \tag{9}$$

This form of the kernel is justified by the spatial isotropy (dependence of k^2 only), normalization ($\hat{K}(0) = \int K(r')dr' = 1$) and locality conditions (rapid decays for $k > 1/d_0$, where d_0 is the characteristic length of the order of electrodes separation). The field dependent factor $\kappa(E)$ describes experimentally observed transitions from honeycombs ($\kappa < 0$) at small fields to coalescence and attraction of toroidal vortices ($\kappa > 0$) for larger fields. After combining Eqs. (6),(8) and (9) one obtains

$$\partial_t V = \nu\nabla^2 V - \zeta V - cE\int K_1(r - r')(\rho_p + \rho_g)dr' \tag{10}$$

where the Fourier transform $\hat{K}_1 = 1 - \exp[-\kappa(E)k^2 - k^4 d_0^4]$. We also scaled away s.

The function f has a different structure for low concentrations ($c \ll 1$) and high concentrations. For $c \to 0$ this function coincides with that derived in Ref. [4]:

$$f_1 = (\rho_p - \rho_*)\times\begin{cases}\rho_p, & \text{if } 0 \le \rho_p \le \rho_* \\ C_*\rho_g(1 - \rho_p), & \text{if } \rho_* \le \rho_p \le 1\,.\end{cases} \tag{11}$$

where constants $C_* \sim O(1)$ and $\rho_*(E)$ are discussed in Ref. [4]. For higher values of c the experiment suggests that both ρ_g and ρ_p tend to some equilibrium value which

is determined by the field E. In the linear approximation it can be written as

$$f_2 = cC_2(\rho_g - \mu(E,q)\rho_p) \tag{12}$$

Here C_2 characterizes relaxation time towards the equilibrium. In steady-state f_2 enforces the relation between the densities $\rho_g/\rho_p \to \mu$. In turn, μ depends on the field and local charge distribution q. We set for simplicity $q = const$. However, convective flows will affect the ions density, which will shift the gas/precipitate equilibrium, see [5]. This effect can be modelled by including the dependence of μ on V. We used the following expression $\mu = \mu_0(E)(\tanh(\mu_1 \mathrm{sign}(E)V) + 1)$. The particular form of this function appears to be not relevant. It incorporates the observation that gas concentration is suppressed by rising flows for $E < 0$ due to excess of negative ions and vise versa. Finally, we used hybrid form for f valid for arbitrary c

$$f = f_2 + \exp[-c/c_0]f_1 \tag{13}$$

where c_0 is some "crossover" concentration.

Stability of homogeneous precipitate. In the limit of small electric fields E we can set $\mu \to 0$, i.e. equilibrium gas density $\rho_g \to 0$. Then the stability of homogeneous precipitate (i.e. homogeneous "Wigner" crystal state in experiment) $\rho_p = \bar{\rho} = const$ can be readily performed because the equation for ρ_g splits off and the analysis is reduced to Eq. (10) and Eq. (1) for ρ_p. We will focus on the case of high concentration $c \gg c_0$ and neglect the last term in Eq. (13) (case of $c = 0$ was considered in Ref. [4]). In the linear order for periodic perturbations $V, \rho_p \sim \exp[\lambda t + ikx]$ Eqs. (1), (10) yield

$$\begin{aligned} \lambda V &= -(\nu k^2 + \zeta)V + E(1 - \exp[-\kappa(E)k^2 - k^4 d_0^4])\rho_p \\ \lambda\rho_p &= -D_p k^2 \rho_p - \alpha_p \beta\bar{\rho}(1 - \beta\bar{\rho})V \end{aligned} \tag{14}$$

The growth rate $\lambda(k)$ depends on the sign of the field E, see Figure 1. For negative E and $\kappa < 0$ in a certain parameter range λ is positive in a narrow band near the optimal wavenumber k_0, which is the hallmark of so-called short-wave instability. In this regime our solution indicates formation of stable honeycomb lattice with the scale determined by k_0. For the same parameters, but for $E > 0$ the homogeneous state $\rho_p = \bar{\rho}$ is stable (dashed line on Figure 1). This observation is consistent with experimental fact that field reversal transforms honeycomb to homogeneous precipitate and vise versa. With the increase of E and κ the left edge of the unstable band of $\lambda(k)$ crosses zero and long-wave instability ensues. This regime corresponds to the coalescence of clusters.

Qualitative phase diagram is shown in Figure 2. The positions of transition lines are approximate because field dependence of κ, μ_0, β is not available at the moment. To describe the observed phenomenology, we only assumed that κ, μ_0, ρ_* monotonically increase with the increase of E, and the functions $\alpha_{g,p}, \beta$ decreases ($1/\beta$ is limiting density of the t-vortex which increases with the increase of E). The line $\lambda = 0$ for short-wavelength instability for $E < 0$ depicts the transition to honeycombs. The transition from honeycombs to pulsating rings is identified as a transition from shortwave to long-wave instability, which roughly coincides with $\kappa(E) = 0$. This transition is associated with an overall increase of gas concentration (increase of $\mu(E)$) and decrease of β (increase of maximum density of ρ_p). The transition from static clusters to dynamic structures and honeycombs occurs approximately with the increase of concentration c at $c = c_0$. For $E > 0$ the transition from stable precipitate to "down t-vortices" is approximately given by $\kappa(E) = 0$. Note that in this case there is no distinction between "immobile" and "Wigner crystal" state because our model does not take into account dry friction and adhesion of particles to the bottom.

Numerical solution of Eqs. (10),(1) was performed by quasi-spectral method based on Fast Fourier Transformation (FFT). Typically 256×256 FFT harmonics in periodic boundary conditions were used. For $c > c_0$, $E < 0$ and $\kappa < 0$ corresponding to the case of short-wavelength

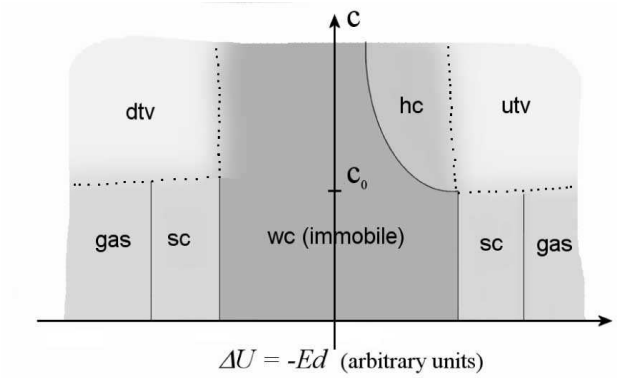

FIG. 2: Qualitative phase diagram, $\Delta U = -Ed$ is applied voltage (plus on top plate), c is concentration of additive. Domain **sc** denotes static clusters, **wc** denotes stable homogeneous precipitate (Wigner crystals), **hc** -honeycombs, **utv** and **dtv** up/down toroidal vortices.

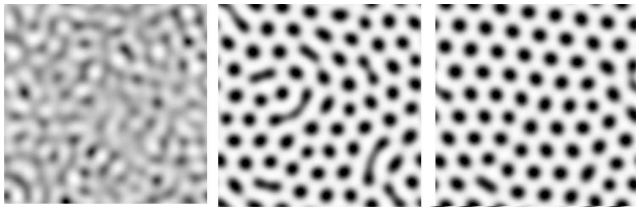

FIG. 3: Formation of honeycomb, shown snapshots of ρ_p, for $\bar{\rho} = 0.3, \nu = 2, E = -50, \alpha = 0.02, \mu_0 = 0, C_1 = 5, c = 1, c_0 = 0.1, C_* = 10, D_p = 1, d_0 = 1, \alpha_p = -\alpha_g = -0.6, \kappa = -0.1, \beta = 2$, domain of integration 80×80 dimensionless units. Images from left to right: t=10; 400; 2000. Black corresponds to $\rho_p = 0$, white to $\max(\rho_p)$.

FIG. 4: Evolution of pulsating rings, shown snapshots of ρ_p, for $\bar{\rho} = 0.18, \nu = 2, E = -70, \alpha = 0.02, \mu_0 = 0.25, \mu_1 = 0.5, C_1 = 5, c = 1, c_0 = 0.1, C_* = 10, D_p = 1, D_g = 5, d_0 = 1, \alpha_p = -\alpha_g = -0.15, \kappa = 0.1, \beta = 0.5$, domain of integration 80×80 units. Images from left to right: t=450; 1120; 3000.

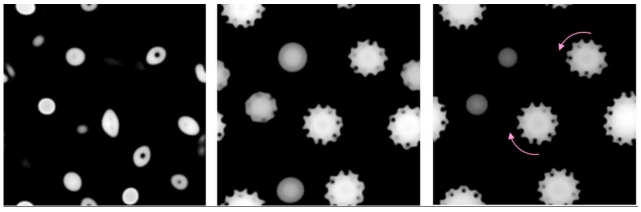

FIG. 5: Rotating down t-vortices, shown snapshots of ρ_p, for $\bar{\rho} = 0.18, \nu = 2, E = 160, \alpha = 0.02, \mu_0 = 19.5, \mu_1 = 0.5, C_1 = 0.45, c = 1, c_0 = 0.1, C_* = 10, D_p = 1, D_g = 5, d_0 = 1, \alpha_p = -\alpha_g = -0.15, \kappa = 0.1, \beta = 0.5$, domain of integration 150×150 units. Images from left to right: t=16; 320; 540.

instability we observed spontaneous formation of honeycomb lattice from random initial conditions, see Figure 3. For the same parameters but $E > 0$ the homogeneous state $\rho_p = const$ (Wigner crystal) was stable. With the increase of E and for $\kappa > 0$ (i.e. in the case of long-wavelength instability) we observed the transition from honeycombs/Wigner crystals to the regime of cluster attraction and coalescence. In this case EHD flows accelerate coarsening process of t-vortices dramatically. The inter-vortex distance R in this regime vs time is shown in Figure 1, inset. The fitting gives approximately $R \sim (t_0 - t)^{1/2}$. It is qualitatively consistent with experimental data. This behavior can be anticipated from solution of Eq. (7). In 2D t-vortices generate localized distributions of vertical velocity V, and, therefore, logarithmic quasipotentials $\Phi \sim \log|\mathbf{r} - \mathbf{r}_i|$, r_i is the vortex position. Thus, the asymptotic horizontal velocity will decay as $V_\perp \sim 1/|\mathbf{r} - \mathbf{r}_i|$ leading to $R \sim (t_0 - t)^{1/2}$.

In the course of coalescence the vortices grow and become unstable, producing pulsating rings for $E < 0$ (Figure 4) and rotating objects for $E > 0$ (Figure 5). We believe that the instability in both cases is caused by the same mechanism: dynamic coupling between particles density and vertical flows described by the function f. However, for $E < 0$, i.e for utv, the vortices are primarily built of a low-mobile precipitate phase with a small amount of gas above them. The instability occurs in the bulk of the vortex, resulting in formation and breaking up of "gas bubbles" inside the precipitate. For $E > 0$ the vortices are formed by a mobile gas phase with a small content of precipitate. The instability occurs at the vortex edge yielding counter-propagating clock/anticlock waves of shape deformation. Eventually only one wave survives, creating the effect of rotation.

In our experiments we observed also multi-petal vortices exhibiting almost solid-state rotation. These multipetal vortices obviously generate horizontal flow of the liquid which is neglected in the framework of our theory. We believe that vertical vorticity is in fact the consequence rather than the reason of rotation. It is likely that the vortex shape instability present in our model eventually triggers rotation of surrounding fluid and generates vertical vorticity. Explicit incorporation of the vertical vorticity will lead to substantial technical difficulties and likely will not change the qualitative features.

In conclusion, we develop phenomenological continuum theory of pattern formation and self-assembly of metallic microparticles immersed in a poorly conducting liquid. This theory reproduces primary patterns observed in the experiment, and leads to an interesting prediction of the relation of rotation with the vortex edge instability. The parameters of the model can be extracted from molecular dynamics simulations and generalization of "leaky dielectric model" [7] and validated by experiments. We are grateful to B. Meerson, Y. Tolmachev and W.-K. Kwok for useful discussions. This research was supported by the US DOE, grant W-31-109-ENG-38.

[1] R.C.Hayward, D.A. Saville, and I.A. Aksay, Nature **404**, 56(2000); M. Trau et al, Nature **374**, 437 (1995); S.-R. Yeh, M. Seul, and B.I. Shraiman, Nature **386**, 57 (1997).
[2] R. B. M. Schasfoort et al, Science, **286**, 942 (1999); A.R. Minerick, A.E. Ostafin, and H.-C. Chang, Electrophoresis, **23**, 2165 (2002)
[3] I.S. Aranson et al, Phys. Rev. Lett. **84**, 3306 (2000)
[4] I.S. Aranson, B. Meerson, P.V. Sasorov, and V.M. Vinokur, Phys. Rev. Lett. **88**, 204301 (2002)
[5] M. V. Sapozhnikov, Y. V. Tolmachev, I. S. Aranson, and W.-K. Kwok, Phys. Rev. Lett. **90**, 114301 (2003)
[6] J.F. Richardson and W.N. Zaki, Trans. Inst. Chem. Eng. **32**, 35 (1954); C.Y. Wen and Y.H. Yu, Chem. Eng. Prog. Symp. Ser. **62**, 100 (1966)
[7] D.A. Saville, Annu. Rev. Fluid Mech, **29**, 27 (1997)